Superparamagnetic Nanocomposites Obtained by Dispersion of Ultrafine Magnetic Iron Oxide Nanoparticles in Poly(3-hydroxybutyrate)

David D'Amico, Laura A. Fasce, Cristina E. Hoppe, M. Arturo López-Quintela, Viviana P. Cyras

PII: S0014-3057(14)00113-X
DOI: http://dx.doi.org/10.1016/j.eurpolymj.2014.03.033
Reference: EPJ 6409

To appear in: *European Polymer Journal*

Received Date: 20 December 2013
Revised Date: 25 March 2014
Accepted Date: 30 March 2014

Please cite this article as: D'Amico, D., Fasce, L.A., Hoppe, C.E., Arturo López-Quintela, M., Cyras, V.P., Superparamagnetic Nanocomposites Obtained by Dispersion of Ultrafine Magnetic Iron Oxide Nanoparticles in Poly(3-hydroxybutyrate), *European Polymer Journal* (2014), doi: http://dx.doi.org/10.1016/j.eurpolymj.2014.03.033

Superparamagnetic Nanocomposites Obtained by Dispersion of Ultrafine Magnetic Iron Oxide Nanoparticles in Poly(3-hydroxybutyrate)

David D'Amico,† Laura A. Fasce, † Cristina E. Hoppe,†, M. Arturo López-Quintela and Viviana P. Cyras†,**

† Instituto de Investigaciones en Ciencia y Tecnología de Materiales (INTEMA), Universidad Nacional de Mar del Plata, Consejo Nacional de Investigaciones Científicas y Técnicas (CONICET), Juan B. Justo 4302, 7600, Mar del Plata, Argentina.

Departamento de Química Física, Facultad de Química, Universidad de Santiago de Compostela (USC), 15782, Santiago de Compostela, España.

***Corresponding author:** Cristina E. Hoppe and Viviana P. Cyras

ABSTRACT

Superparamagnetic nanocomposites were obtained by dispersion of oleic acid-coated magnetic ultrafine iron oxide nanoparticles (NPs) in poly(hydroxybutyrate) (PHB), a semicrystalline, biodegradable and biocompatible polymer. Film nanocomposites displayed an optically homogeneous structure formed by sub-micrometric clusters created by a strong NPs segregation that occurred during solvent evaporation and polymer crystallization. Number and size of clusters increased with the concentration of NPs producing a controlled shift in the blocking temperature but hardly affecting PHB crystallinity and melting temperature. The presence of NPs decreased the elastic modulus of PHB and slightly reduced its hardness, leading to materials with improved resistance to permanent damage. This softening effect was attributed to the oleic acid shell covering the iron oxide core of the NPs. The present results shed some light on the mechanisms controlling morphology of semicrystalline-based nanocomposites modified with ultrafine NPs, opening interesting possibilities for the design of materials with controlled functional properties.

Keywords: Biodegradable Polymers, Poly(hydroxybutyrate), Superparamagnetic Materials, Nanocomposites.

INTRODUCTION

The design of polymer nanocomposites with predictable properties is a challenge that requires an efficient way to control the dispersion level of the nanoparticles (NPs) in the host matrix and a deep understanding concerning how these structures affect the final properties of the materials [1-5]. While it is well accepted that NPs dispersion strongly affects nanocomposites properties, it is not clear that a single state of dispersion or arrangement should optimize any given or all macroscale properties [5]. Sometimes, even

the presence of NPs aggregates could be required in a solid material or colloidal dispersion for a specific function or property optimization [6]. The use of gold NPs aggregates as efficient photothermal heaters [7] and the application of stable colloidal aggregates formed by the assembly of individual magnetic NPs in MRI imaging [8] are some examples that prove the importance of the formation of aggregates in the design of new applications. In a similar way, both catalytic and optical properties [9] can be enhanced through the formation of controlled NPs aggregates. These effects are a consequence of the strong influence that magnetic and dipolar interactions between particles have on the properties of final assemblies and show that aggregates are not always a problem but can be used as a design strategy for the synthesis of films with new and specific properties. Chemical affinity, polymer crystallinity, polymer crystallization kinetics, size and shape of NPs and relative sizes of these nanostructures respect to the polymer gyration radius, as well as processing conditions, can profoundly influence the level of dispersion attained [1-5]. Thus, relationship between all the variables of the fabrication processes and final states of NPs dispersion are important issues at the time of controlling reproducibility and material behaviour for a specific function.

Compared with the preparation of materials based on amorphous polymers, dispersion of NPs in semicrystalline hosts is linked to the control of much more variables. Presence of a crystalline phase limit the location of modifiers (polymers, NPs, etc.) to the amorphous region (interspherulitic, intraspherulitic or interlamellar regions) [10-11] decreasing the available volume for NPs incorporation and making the morphology of these nanocomposites very dependent on the crystalline degree of the host, kinetic of crystallization and processing conditions (crystallization kinetics, annealing steps, presence

of solvent, etc.) [12-13]. This idea was first reported by Kahn et al., which studied the effect of crystallization on the dispersion of small PMMA coated silica NPs (15 nm) in PEO and found a behaviour that resembles that of molecular systems, in which the host "push" impurities out of the way of the crystal to maintain the crystallization process minimally perturbed [14]. They compared crystallization of nanocomposites formed by small NPs with crystallization behavior of polymer blends with a crystallizable and an amorphous component in which, for slow enough crystallization rates, the amorphous polymer can be completely expelled from the spherulites. This is not the common result found in the case of polymer nanocomposites synthesized with platelet fillers or large micrometer sized particles, too large to be easily maneuvered by the growing lamellae.

From the opposite point of view, the presence of NPs can affect crystallinity, lamellar thickness, spherulitic size and even crystalline structure of polymers, which are expected to have an important impact on mechanical and barrier properties and on chemical resistance of final materials [15-16]. In this regard, different and controversial effects have been reported. Larger crystallinity degrees have been produced thanks to an enhanced crystallization ability of the matrix in the presence of nanofillers, which behave as nucleating agents. Mitchell and Krishnamoorti [17] reported that for the carbon nanotubes/poly(ε-caprolactone) composite systems the nucleation activity was approximately 0.56, thus it can deduced that the nanotubes incorporation acts as a source of heterogeneous nucleation sites. On the other hand, a decrease of the percentage of crystallinity with the increase in NPs content has been produced as a consequence of partial inhibition on polymer crystal formations [14, 18-20]. To further complicate this picture, recent reports have shown that moderate loadings of small NPs could have a negligible

effect on crystallinity and melting temperature of highly crystalline polymers [22, 23]. Therefore, under this complex scenario, the analysis of the inter-relationship between processing, morphology and properties of nanocomposites based on semicrystalline polymers is of fundamental interest for scientists and technologists and it requires a deep research.

Modification of biocompatible polymers with inorganic nanostructures opens interesting possibilities for the development of new materials [24-26]. For example, the modification of highly semicrystalline biodegradable polymers, like Poly(3-hydroxybutyrate) (PHB), poly(L-lactic acid) (PLLA) and poly(ethylene oxide) (PEO) with functional nanostructures, opens a broad range of potential applications in the biomedical field [24].

In particular, PHB is a biodegradable polyester, synthesized and intracellularly stored by several microorganisms in the form of granules, with properties that make it suitable for many applications in which petroleum-based synthetic polymers are currently used [27]. PHB can be produced from renewable sources through fermentation processes under restricted growth conditions [28]. It is a thermoplastic polymer with a high degree of crystallinity and with physical and mechanical properties close to those of isotactic polypropylene [28].

In this work, we evaluate the possibility of obtaining magnetic nanocomposites with reproducible and predictable properties, starting from PHB and ultrafine iron oxide NPs coated with oleic acid, one of the most common organic coatings used in the synthesis of iron oxide NPs [29]. We focus the investigation on the mechanisms that control dispersion of ultrafine NPs in highly crystalline nanocomposites as well as on the influence that their

arrangement has on magnetic, thermal and mechanical properties. To this aim some of the results of PHB/iron oxide NPs are compared with those of a similar system (PEO/iron oxide NPs).

EXPERIMENTAL

Materials

Poly(3-hydroxybutyrate) (PHB) (kindly supplied by PHB Industrial S. A., Brazil, Mv≈ 250 000) and Poly (ethylene oxide) (PEO), with a molecular weight, Mw ≈ 300 000 (Aldrich) were used as polymeric hosts. PEO was used for comparative purposes in magnetic measurements. Ferric chloride ($FeCl_3.6H_2O$), ferrous sulphate ($FeSO_4.7H_2O$), cyclohexane, dichlorometane, chloroform, poly-oxyethylen-10-oleyl ether (Brij-97), oleic acid and oleylamine were purchased from Aldrich and used to prepare NPs and films. All the reagents of analytical grade were used as received. Deionized water was used in NPs preparations.

NPs synthesis

Ultrafine magnetite NPs with two different sizes were synthesized in order to study the effect of the size for certain selected formulations. NPs with an average size of 3.5 nm coated with oleic acid (γ-Fe_2O_3@OA-3.5) were obtained by a microemulsion method [30]. In brief, a (cyclohexane/ Brij 97/ aqueous phase) system was used with an aqueous phase formed by a 2:1 ferric-ferrous solution. Oleylamine was added to the microemulsion with magnetic stirring to form NPs. Final stabilization was attained by adding a 50/50 molar mixture of oleic acid and oleylamine on the reaction media. The obtained oleic acid-coated NPs were separated, washed and finally dispersed in chloroform to form a stable ferrofluid.

NPs with an average size of 9.5nm coated with oleic acid (γ-Fe_2O_3@OA-9.5) were obtained by a chemical coprecipitation method [31] followed by stabilization with oleic acid. Briefly, 0.09 mol of $FeCl_3.6H_2O$ and 0.06 mol of $FeSO_4.7H_2O$ were dissolved in 200ml distilled water and heated to 90°C. For precipitation and stabilization, 60 ml of ammonium hydroxide and 0.014 mol of oleic acid were sequentially added rapidly. The black sediment was purified by successive cycles of redispersion and precipitation in heptane and ethanol. Last dispersion cycle was done in chloroform to obtain a stable ferrofluid.

Nanocomposite films preparation

Films of neat polymers and nanocomposites were obtained by a solvent casting process. Selected amounts of a chloroform (for PHB) or dichloromethane (for PEO) dispersion of NPs containing 25 mg of γ-Fe_2O_3@OA per ml were mixed with a solution of 1 g of the polymer in 15 ml of the respective solvent. For PHB systems, homogeneous solutions were prepared by stirring at 450 rpm while heating at 60°C, for 15 minutes. Then, the solution was placed on a 15 cm diameter glass Petri dishes and it was allowed to evaporate at room temperature. All films were stored in a desiccator at room temperature for 30 days to allow complete crystallization of PHB [32]. In the case of PEO systems, a similar procedure was followed without the heating step.

Characterization methods

Transmission electron microscopy (TEM) images were obtained using a Philips CM-12 microscope operated at an accelerating voltage of 100 kV. NPs samples were prepared by dropping 6μL of the dispersion on a copper grid coated with Formvar and a

carbon film. Nanocomposite samples were obtained from ultrathin sections cut with a cryo-ultramicrotome.

Small-angle X-ray scattering (SAXS) measurements were taken at room temperature at the beam line SAXS 1 of the National Laboratory of Synchrotron Ligth (LNLS, Campinas, Brazil). The scattering intensity (in arbitrary units) was recorded as a function of the scattering vector $q = (4\pi/\lambda) \sin\theta$, where λ is the light wavelength (1.55 Å) and 2θ the scattering angle.

X-ray diffraction (XRD) spectra of NPs and nanocomposites were obtained with a PANalyticalX'Pert Pro diffractometer using a CuKα radiation source (λ= 0.1546 nm), operating at 40kV and 40mA. Scherrer equation was used to determine the average crystallite size, from (110) reflection:

$$t = 0.9\,\lambda/(B\cos\theta_B)$$

with λ being the wavelength of the X-rays, B the width of the peaks (in radians) at the half of the maximum intensity and θ_B the angle (in radians) at which the intensity is a maximum.

Thermogravimetric analysis (Shimadzu TGA-50) was carried out on 5mg samples at a heating rate of 10ºC/min under air flow, up to 900ºC. TGA thermograms were used to determine the amount of NPs in the nanocomposites and the fraction of oleic acid coating the NPs.

Differential Scanning Calorimetric (DSC) measurements were carried out in a Shimadzu DSC-50 from room temperature to 200ºC at 10ºC/min, under N_2 atmosphere.

The melting temperature (T_m), melting enthalpy (ΔH_m) and glass transition temperature (Tg) were recorded in the first scan. The polymer crystallinity degree (X_c) was calculated as:

$$X_c(\%) = \frac{\Delta H_m.(m_C / m_P)}{\Delta H_0}.100 \qquad \text{Eq. (1)}$$

where ΔH_m is the experimental melting enthalpy, ΔH_0 is the theoretical enthalpy of 100% crystalline polymer (146 J/g for PHB [33] and 197 J/g for PEO [33]), m_c is the nanocomposite mass and m_p is the polymer mass in the nanocomposite.

Magnetic properties of nanocomposite films were measured between 5K and 300K in a Quantum Design PPMS. Experiments were done under zero field cooling (ZFC) and field cooling (FC) conditions at H =100Oe.

Uniaxial tensile experiments were carried out at room temperature in an INSTRON 4467 universal testing machine. Dumb-bell shaped specimens were tested at a crosshead speed of 1mm/min. Stress (σ_b) and strain (ε_b) at break were calculated from the nominal stress–strain curves. Properties were averaged from at least 5 tests.

Depth sensing indentation tests were carried out at room temperature in a Triboindenter Hysitron equipped with a Scanning Probe Microscope module (SPM). Tests were performed under load control conditions using a diamond Berkovich tip. The loading/unloading rate, maximum load (P_{max}) and holding time were respectively 0.3mN/s, 3mN and 15s. The holding period at maximum load was applied to minimize creep effect on unloading curve [35-36]. At least 50 indentations were made in different locations of each sample to reduce the scattering arisen from surface roughness [37]. Analysis for the

tip area calibration and calculation of contact stiffness (S), reduced elastic modulus (E_r) and indentation hardness (H) were conducted using the approach outlined by Oliver and Pharr [38-39]. The maximum load to contact stiffness squared parameter (P/S^2), which is a measure of the material resistance to permanent deformation, was also evaluated [40-41].

RESULTS AND DISCUSSIONS

Nanocomposites Dispersion

TEM micrographs of the synthesized NPs, with 3.5±0.6 nm and 9.5±2.6 nm of average diameter, are shown in Figure 1. As can be seen, oleic acid coating avoids direct contact between iron oxide cores stabilizing them against aggregation and makes them highly dispersible in organic solvents like chloroform, THF, hexane, etc.

PHB film Nanocomposites were obtained by a slow evaporation casting process from clear dispersions of magnetite NPs in PHB chloroform solutions. Oleic acid-coated magnetite NPs form very stable dispersions in this solvent enabling the efficient mixing of both components and avoiding formation of NPs aggregates previous to evaporation. Slow evaporation rates under solvent atmosphere were used as conditions favouring self-organization of NPs in the polymer matrix and minimization of residual stresses in the films.

Optical photographs of the films with different concentrations of γ-Fe_2O_3@OA-3.5 are shown in Figure 2. As can be seen, final materials were optically homogeneous showing no evidences of NPs macroscopic aggregation. Enhancement in colour intensity (from orange to deep brown) was an expected consequence of the increase in NPs concentration.

Although optical homogeneity of films indicated a good level of NPs dispersion in the matrix, TEM analysis of films nanocomposites revealed the presence of NPs clusters with typical sizes in the order of hundreds of nanometers in all the samples (Figure 3).These clusters are formed by the assembly of individual NPs separated by the oleic acid coating (Fig. 3*e*). TEM observations indicated that mean size of aggregates in all samples was not higher than 200 nm (Feret diameter), except for an intermediate composition corresponding to 7 wt% of NPs, in which some aggregates with sizes up to 450 nm could be found (Table 1). This non-intuitive result could be explained in terms of changes in NPs concentration and viscosity of the medium during formation of films. It has been recently proposed that in nanocomposites obtained with very small NPs (like those used in this work), crystallization dominates organization of NPs, pushing them out of the way so as to result in a minimally perturbed crystallization process [23].

In this framework it seems reasonable that final distribution of particles will depend on variables like initial NPs concentration and viscosity of the medium, both affecting probability of particle-particle encountering. At low concentrations, viscosity of the medium is not very high so NPs can be easily handled by the growing lamellae and expelled to intra, interfibrillar or interspherulitic regions where they could find each other to form submicrometric assemblies. In this case, size of the aggregates would be limited by the number of nearest particles that can join each other before crystallization completes. At the highest loadings, although NPs are much closer each other, viscosity is also much higher. Very high viscosities would decrease the diffusion rate of NPs, hampering further growth of aggregates before crystallization and producing a decrease in their mean size. This picture could explain the existence of a maximum in aggregate size located at

intermediate loadings (in this case around 7 wt. %) corresponding to an optimum scenario of relatively high concentration and low viscosity.

A certain degree of orientation in the way NPs assembled can also be inferred from TEM micrographs, especially at high loadings (Figure 3 *c* and *d*). They show formation of non-spherical clusters with their long axis pointing along a preferential direction. The origin of this effect is still not clear but could be attributed to a sort of "template" effect of lamellae, suggesting that formation of clusters occurred during the advance of crystallization front, by rejection of NPs outside the developing crystal.

Formation of aggregates was also confirmed by SAXS for all analysed samples (Figure 4). In these spectra the origin of the scattering peaks is associated with the dominant electron density contrast between iron oxide and the polymer. Films prepared with 3.5 nm NPs showed broad interference peaks centred at q values of about 1.1-1.2 nm^{-1} corresponding to characteristic lengths $d=2\pi/q$, between 5.7-5.2 nm, respectively. Discounting a distance of about 3.5 nm for the iron oxide core leads to an edge-to edge separation between NPs of about 1.7-2.2 nm, which agrees well with typical distances (about 2 nm) observed in compact self-assembled arrangements of oleyl-coated nanostructures in which alkyl chains are inter-digitated. This shows a high degree of confinement for these NPs loadings. Slight differences observed in the position of the scattering peaks for different iron oxide contents could be a consequence of subtle variations in the degree of compactness of aggregates. Similar conclusions were obtained for samples prepared with bigger NPs (mean size = 9.5 nm). In this case, the scattering peak centred at $q=0.55$ nm^{-1} corresponded to d = 11.4 nm and a mean edge-to edge

separation of about 1.9 nm. In all cases, broadness of the peaks suggests no regular order in the aggregates, indicating that NPs are forming random arrangements with a quite broad distribution of interparticle distances. Is interesting to note that these are shorter distances when compared with that found between silica particles by Kahn et al. in PEO nanocomposites [14]. This is probably a consequence of the different nature of the NPs coating (a PMMA oligomer for silica and an oleic acid chain in the case of iron oxide used by us) and the dynamic of segregation, controlled by competition between viscosity and crystallization rate.

Formation of submicrometer clusters of NPs in semicrystalline polymers have also been reported in the recent literature for systems obtained at slow evaporation conditions [42]. Hence, in the case of ultrafine particles, formation of more homogeneous nanocomposites seems to be restricted to fast cooling from the melt, fast evaporation of solvent or post-synthesis processes that minimize diffusion of NPs and growing of aggregates, freezing non-equilibrium morphologies.

Surprisingly, mean size of aggregates do not seem to strongly depend on the nature of the matrix. NPs clusters of similar size have been reported in samples obtained by dispersion of the same oleic-acid NPs (γ-Fe_2O_3@OA-3.5) in PEO, a very hydrophilic polymer in which aggregation should be favoured as a consequence of chemical incompatibility [42]. This could indicate that for certain range of concentrations, size of aggregates could be more influenced by crystallinity and segregation processes than for chemical compatibility.

Modification of PHB with larger NPs (9.5 nm) hardly changed the morphology of nanocomposites as shown in Figure 5. Clusters with similar sizes and morphologies could be observed in TEM images. This indicates that, at least for moderate loadings, size of NPs has a negligible effect on clusters formation mechanism.

Properties of Nanocomposites

Thermal behaviour of neat films and nanocomposites was analysed by DSC. The calculated percentage of crystallinity (X_c) and the melting temperature at the peak for each material are summarized in Table 2. It is clear from these results that NPs incorporation had little effect on the matrix crystalline degree since the obtained values showed a maximum deviation of only 5% respect to the neat matrix. These results differ from that found by Kahn et al. for PEO/silica systems [14] which reported changes in crystallization degree for increasing NPs loadings. This could be associated with the lower size of iron oxide NPs and the lower crystallinity of PHB respect to PEO used by Kahn et al. (0.64 vs 0.87). In addition, the melting temperature of samples hardly changed with the addition of NPs, indicating also a low effect of NPs content on crystal size. Moreover, only small changes in the average size of crystallites (t), as determined by Scherrer equation, were observed for increasing loadings of NPs (Table 2). Slight influence of NPs on crystallinity, melting temperature and crystal size has been also recently reported for other semicrystalline polymers modified with very fine NPs [43-44]. This would indicate that confinement of NPs to the amorphous zones may occur without significant disturbance of the normal development of crystals in the neat biopolymer. However, subtler effects, like interference on lamellae or bundles arrangement with resulting increases in spherulite disorder, cannot

be discarded at this point. Therefore, we propose that small NPs segregate from the crystal phase during polymer crystallization in interlamellar, inter lamellar-bundle or interspherulitic regions, giving place to the formation of concentrated regions of NPs located in amorphous zones between crystalline domains. Formation of NPs aggregates (typically with sizes well below the micrometer range) are then originated by the increase in local concentration of NPs produced by the advance of the crystallization front and the confinement of NPs into the amorphous regions.

Magnetic Properties

As described above, modification of semicrystalline polymers with superparamagnetic NPs has importance in the development of functional materials with interesting applications in magnetic guiding, bioseparation, drug delivery, etc. Furthermore, analysis of magnetic properties is useful as a characterization tool of the dispersion level of magnetic nanocomposites.

For single domain NPs, the anisotropy energy barrier, E_B, for magnetization relaxation is proportional to the volume. To overcome E_B, a single-domain particle is assisted by thermal phonons. Therefore, below a certain size, thermal energy can overcome E_B and make the whole magnetic moment of the particle to fluctuate above a characteristic temperature, T_B, called blocking temperature. Below T_B the free movement of the moment of the particle is blocked by the anisotropy; above T_B, thermal energy induces rapid fluctuations of the magnetic moment of the whole particle compared to the observation time so that the system appears superparamagnetic. E_B is related to an effective anisotropy constant, K_{eff}, through E_B = Keff .V (where V is the volume of the particle). Magnetic

interactions modify the energy barrier and, in the limit of strong interactions, their effects become dominant becoming the total energy of the assembly the only relevant magnitude [45].

Magnetic properties of PHB films were measured for variable concentrations of NPs. Experiments were done under zero field cooling (ZFC) and field cooling (FC) conditions at H = 100 Oe (Figure 6). A maximum in the curve of ZFC associated to the blocking temperature, T_B, separates the blocked from the Superparamagnetic state. (Figure 6). Magnetization in FC conditions increased with decreasing temperature for both curves, ZFC and FC, splitting from slightly above T_B. This behaviour is characteristic of weakly interacting systems of superparamagnetic NPs. As observed, for higher loadings of NPs the peak broadens, T_B shifts to higher temperatures and low temperature saturation becomes evident in the FC curves, in agreement with a progressive decrease in the NPs distance and an increase in the magnetic dipolar interactions [46].

PHB based nanocomposites showed a magnetic behaviour similar to that reported for PEO nanocomposites prepared with an identical batch of NPs [42] (Figure 7). This could be understood considering the high similarity in the morphology of the NPs distribution (as discussed in the previous section). This behaviour was, nevertheless, very different from that observed for ideally dispersed systems [47-48]. Figure 7 shows the dependence of T_B with the NPs content for PEO, PHB and poly(vinyl butyral), PVB, based nanocomposites. PVB is an amorphous polymer that, with the same oleic acid-coated NPs used in this work, forms ideally dispersed nanocomposites [42]. As clearly seen, T_B values for PHB and PEO nanocomposites were higher than for PVB ones in all the range of

concentrations. Moreover, whereas the dependence of T_B with wt% NPs was similar for PEO and PHB nanocomposites, it strongly differed from that obtained for PVB nanocomposites. Ideally dispersed systems are characterized by a critical concentration value, C*, separating a non-interacting regime (C< C*), in which T_B does not vary with NPs loading, and an interacting regime (C> C*), in which the dipolar energy enhances the anisotropic energy barrier and T_B increases with increasing concentration [48]. The strong dependence of T_B with loading found for PHB and PEO systems evidenced the contribution of strong magnetic dipolar interactions to the magnetic behaviour, even at low concentrations of NPs. These results could be understood by the presence of regions of high NPs concentration (clusters) in which NPs are in close proximity and dipolar interactions are not negligible. This contribution would be responsible for the shifting and broadening of the ZFC curves hampering the observation of the non-interacting regime [48].

The most interesting point of this analysis is the fact that samples formed by sub-micrometer clusters follow a clear and reproducible behaviour in their magnetic response. It is common to connect NPs aggregation processes with unpredictable and random behaviour of final materials. However, in this case, crystallization seems to work by imposing a restriction to growing of aggregates in a quite controlled way. An increase in NPs concentration produces an increase in the number of aggregates with its consequent effect on magnetization, blocking temperature and broadness of the peak that seems to follow a similar trend quite independently of the chemical nature of the semicrystalline matrix. Finally, T_B and peak broadening were observed in samples prepared with bigger NPs, which can be easily explained by the increase in anisotropy and strength of dipolar interactions expected for higher NPs volumes (Figure 8).

Mechanical Behaviour

Mechanical behaviour of the prepared nanocomposites films was investigated by performing uniaxial tensile and depth sensing indentation experiments. Typical mechanical responses are shown in Figure 9a while a selection of mechanical parameters is listed in Table 3.

Under uniaxial tensile conditions PHB films behaved in a brittle manner exhibiting catastrophic failure at relative low deformation levels (typically less than 1%) (Figure 9a). The incorporation of γ-Fe_2O_3@OA unaltered the inherent brittle nature of the matrix behaviour. The addition of 3wt% of γ-Fe_2O_3@OA-3.5 promoted a reduction in the elastic modulus and slight increase in the strain at break. Further NPs incorporation, at least in the studied concentration range, had little effect on nanocomposites stiffness but reduced the maximum deformation capability. Given that PHB crystallinity was practically unchanged by the presence of NPs, the reduction in elastic stiffness can be explained by the structure of the NPs (or aggregates). A hard Fe_2O_3 core is coated with a soft oleic acid shell, so that aggregates were mechanically seen by the matrix as soft modifier particles. However, a decreasing trend in elastic modulus with increasing NPs concentration was not observed, probably due to the complex distribution of NPs.

Unlike under uniaxial tension, all materials were able to develop plastic deformation under indentation load because the stress field beneath the indenter is mainly compressive, so that failure mechanisms, such as crazing, that promotes brittle fracture are suppressed. This was reflected in the loading/unloading curve hysteresis (Fig 9b), which is indicative of

irreversible deformation. The incorporation of NPs slightly changed the indentation response of the PHB matrix.

As discussed above, the presence of NPs decreased the stiffness of the films. The reduced indentation modulus, E_r, decreased with increasing NPs content. As well, indentation hardness, H, which is directly proportional to yield stress, [49] showed a slight decreasing trend with NPs content. The elastic stiffness, S, decreased in a larger extent than yield stress so that the P/S^2 parameter increased, indicating that the nanocomposites turned out to be more resistant to permanent deformation than PHB.

In summary, our results indicate that the addition of well dispersed $\gamma Fe_2O_3@OA\text{-}3.5$ slightly improved the mechanical behavior of PHB. The enhanced resistance to permanent damage may be linked to the interaction of core-shell NPs with growing crazes in the amorphous regions as described by Lee et al. [50]. They suggest that even NPs do not prevent craze fibrils formation, a new damage microstructure containing NPs clusters entrapped within the mature crazes is formed by local alignment and repulsion of the particles.

CONCLUSIONS

Reproducible superparamagnetic nanocomposites formed by sub-micrometric NPs clusters dispersed in a semicrystalline, biodegradable and biocompatible polymer, PHB, could be obtained by a casting technique.

The crystallinity and lamellar thickness of the polymeric matrix were not importantly affected by the presence of NPs as a consequence of segregation of NPs to the

amorphous phase. Formation of clusters could be originated by the increase in local concentration of NPs produced by the advance of the crystalline phase and confinement of NPs to the amorphous phase.

Progressive increase in the blocking temperature of nanocomposites for variable amounts of magnetic NPs pointed to a behaviour mainly controlled by the number and size of dispersed clusters. Concentration of NPs in these aggregates was limited by the oleic acid coating used to stabilize NPs which enabled to maintain their individuality, helping to preserve the superparamagnetic state.

Mechanical behaviour of PHB was slightly improved by the incorporation of the NPs. The dispersed clusters act as soft-shell particles and nanocomposites turned out to be less stiff but more resistant to permanent deformation than PHB.

Our results show that morphology of the NPs distribution, at least for this size of the NP core, was strongly controlled by crystallinity of the matrix and processing conditions and that chemical nature of the matrix had little influence on the size and shape of aggregates and, consequently, on final properties of the materials. Both the slight increase in the resistance to permanent deformation of nanocomposites respect to the pristine polymer and the progressive change of the blocking temperature for variable amounts of NPs constitute new and valuable results proving that presence of aggregates did not preclude the generation of well controlled, high performance superparamagnetic nanocomposites.

ACKNOWLEDGMENT

The financial support of the following institutions is gratefully acknowledged: National Research Council (CONICET, Argentina, PIP 0014/10), National Agency for the Promotion of Science and Technology (ANPCyT, Argentina, PICT010-1008) and University of Mar del Plata, (15/G336, 15/G369 and 15/G374). The grant SAXS1-13459 from the Brazilian Synchrotron Light Laboratory (LNLS, Campinas-SP, Brazil), is gratefully acknowledged. The authors specially thank to Prof. Francisco Rivadulla Fernández (Ciqus-University of Santiago de Compostela, Spain) for valuable help with magnetic measurements and to the whole staff of the SAXS line 1 (LNLS, Campinas) for support with SAXS measurements.

REFERENCES

1- Rozenberg BA, Tenneb R. Prog Polym Sci 2008; 33: 40–112.

2- Zhang H, Han J, Yang B. Adv Funct Mater 2010; 20: 1533–1550.

3- Vaia RA, Maguire JF. Chem Mater 2007; 19: 2736.

4- Cyras VP, Manfredi LB, Ton-That MT, Vázquez A. Carbohydr Polym 2008; 73: 55-63.

5- Jancar J, Douglas JF, Starr FW, Kumar SK, Cassagnau, P, Lesser J, Sternstein SS, Buehle MJ. Polymer 2010; 51: 3321-3343.

6- Skirtach AG, Déjugnat C, Braun D, Susha AS, Rogach AL, Sukhorukovr GB. J Phys Chem C 2007; 111: 555-564.

7- Sanchot A, Baffou G, Marty R, Arbouet A, Quidant R, Girard C, Dujardin E. ACS Nano 2012; 6: 3434–3440.

8- Larsen BA, Haag MA, Serkova NJ, Shroyer KR, Stoldt CR. Nanotechnology 2008; 19: 265102.

9- Liu Y, Zhang Y, Ding H, Xu S, Li M, Kong F, Luo Y, Li G. J Mater Chem A 2013; 1: 3362-3371.

10- Ma D, Akpalu YA, Li Y, Siegel RW, Schadler LS. J Polym Sci, Part B: Polym Phys 2005; 43 : 488–497.

11- Hudson S D, Davis D D, Lovinger A J Macromolecules 1992; 25: 1759-1765.

12- Kaur J, Hoon Lee J, Bucknall DG, Shofner ML. ACS Appl Mater Interfaces 2012; 4: 3111−3121.

13- Kaur J, Hoon Lee J, Shofner ML. Polymer 2011; 52: 4337-4344.

14- Khan J, Harton SE, Akcora P, Benicewicz BC, Kumar SK. Macromolecules 2009; 42: 5741–5744.

15- Chatterjee T, Lorenzo AT, Krishnamoorti R. Polymer 2011; 52: 4938-4946.

16- Hoon Lee J, Shofner M L. Polymer 2012; 53: 5146-5154.

17- Mitchell CA, Krishnamoorti R. Polymer 2005; 46: 8796–804.

18- D'Amico DA, Manfredi LB, Cyras VP. Thermochim Acta 2012; 53: 544- 547.

19- Bhatt AS, Denthaje Krishna Bhat DK. Mater Sci Eng B 2012; 177: 127-131.

20- Suthanthiraraj SA, Vadivel MK. Appl Nanosci 2012; 2:239–246.

21- Modi SH, Dikovics KB, Gaurav Mago HG, Bartolucci SF, Fisher FT, Kalyon DM. Polymer 2010; 51: 5236-5244.

22- Crétois R, Delbreilh L, Dargent E, Follain N, Lebrun L, Saiter JM. Eur Polym J 2013; 49: 3434-3444.

23- D'Amico DA, Manfredi LB, Cyras VP, Journal of Applied Polymer Science, 2012; 123: 200-208.

24- Yang L, Zhang L, Webster T. J Adv Eng Mater 2011; 13: 197-217.

25- Shchipunov Y. Pure Appl Chem 2012; 84: 2579–2607.

26- Aimé C, Coradin T. J Polym Sci, Part B: Polym Phys 2012; 50: 669–680.

27- Michalak M, Marek A,; Zawadiak J, Kawalec M, Kurcok P. Eur Polym J 2013; 49: 4149-4156.

28- Chatzidoukas CH, Penloglou G, Kiparissides C. Biochem Eng J 2013; 71: 72-80

29- Gage SH, Stein BD, Nikoshvili LZh, Matveeva VG, Sulman MG, Sulman EM, Morgan DG, Yuzik-Klimova EYu, Mahmoud WE, Bronstein LM. Langmuir 2013; 29: 466–473.

30- Vidal-Vidal J, Rivas J, López-Quintela MA. Colloid Surf A - Physicochem Eng Asp 2006; 288: 44-51.

31- Zheng W, Gao F, Gu H. J Magn Magn Mater 2005; 288: 403–410.

32- Puppi D, Chiellini F, Piras, AM, Chiellini E. Prog Polym Sci 2010; 35: 403–440.

33- Mitomo H, Watanabe Y, Ishigaki I, Saito T. Polym Degrad Stab 1994; 45: 11-17.

34- Buckley CP, Kovacs A. J Prog Colloid Polym Sci 1975; 58: 44–52.

35- Geng KB, Yang FQ, Druffel T, Grulke EA Polymer 2005; 46: 11768-11772.

36- Ngan AH W, Tang B. J Mater Res 2002; 17: 2604-2610.

37- Berke P, El Houdaigui F, Massart TJ. Wear 2010; 268: 223–232.

38- Oliver WC, Pharr GM. J Mater Res 1992; 7: 1562-1584.

39- *International standard ISO 14577*-1. 2002. Metallic materials — Instrumented indentation test for hardness and materials parameters.

40- Joslin DL, Oliver WC. J Mater Res 1990; 5: 123-126.

41- Fasce L, Costamagna V, Pettarin V, Strumia M, Frontini P. Express Polym Lett 2008; 2: 779-790.

42- Hoppe CE, Rivadulla F, López-Quintela MA, Buján MC, Rivas J, Serantes D, Baldomir D. J Phys Chem C, 2008; 112: 13099–13104.

43- Xie, Y., Kohls, D., Noda, I., Schaefer, DW, Akpalu YA. Polymer 2009; 50, 4656–4670.

44- Huang X., Jiang P., Kim C, Duan J, Wang G. J Appl Polym Sci 2008, ; 107 : 2494–2499.

45- Batlle X, Labarta AJ Phys D: Appl Phys 2002; 35: R15–R42.

46- Prend P, Tronc E, Jolivet J, Livage J, Cherkaoui R, Noguks M, Dormann J, Fiorani D. IEEE Trans Magn 1993; 29: 2658-2660.

47- Hoppe CE, Rivadulla F, Vidal-Vidal J, López-Quintela MA, Rivas J Nanosci Nanotechnol 2008; 8: 2883-2890.

48- Serantes D, Baldomir D, Pereiro M, Hoppe CE, Rivadulla F, Rivas J. Phys Rev B 2010; 82: 134433.

49- Fischer-Cripps, AC Introduction to Contact mechanics, 2nd Ed., Springer, New York, 2007.

50- Lee J-Y, Zhang Q, Emrick T, Crosby AJ. Macromolecules 2003; 39: 7392-7396A.

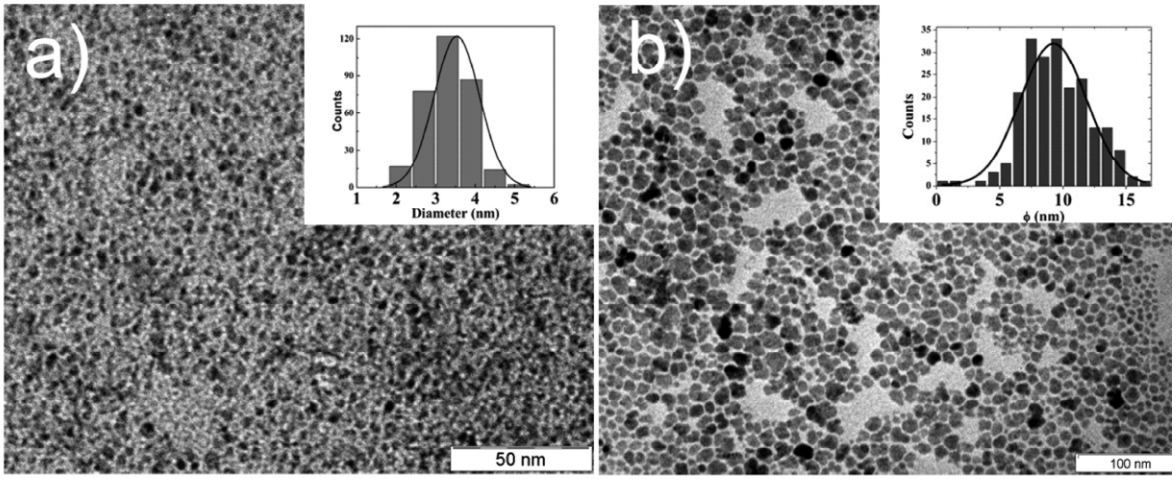

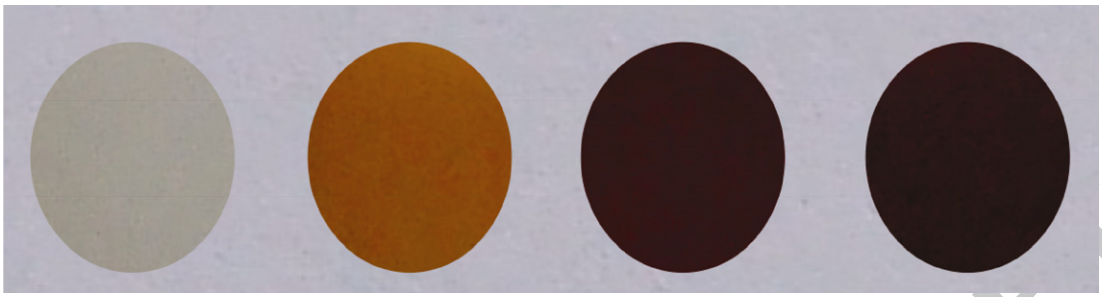

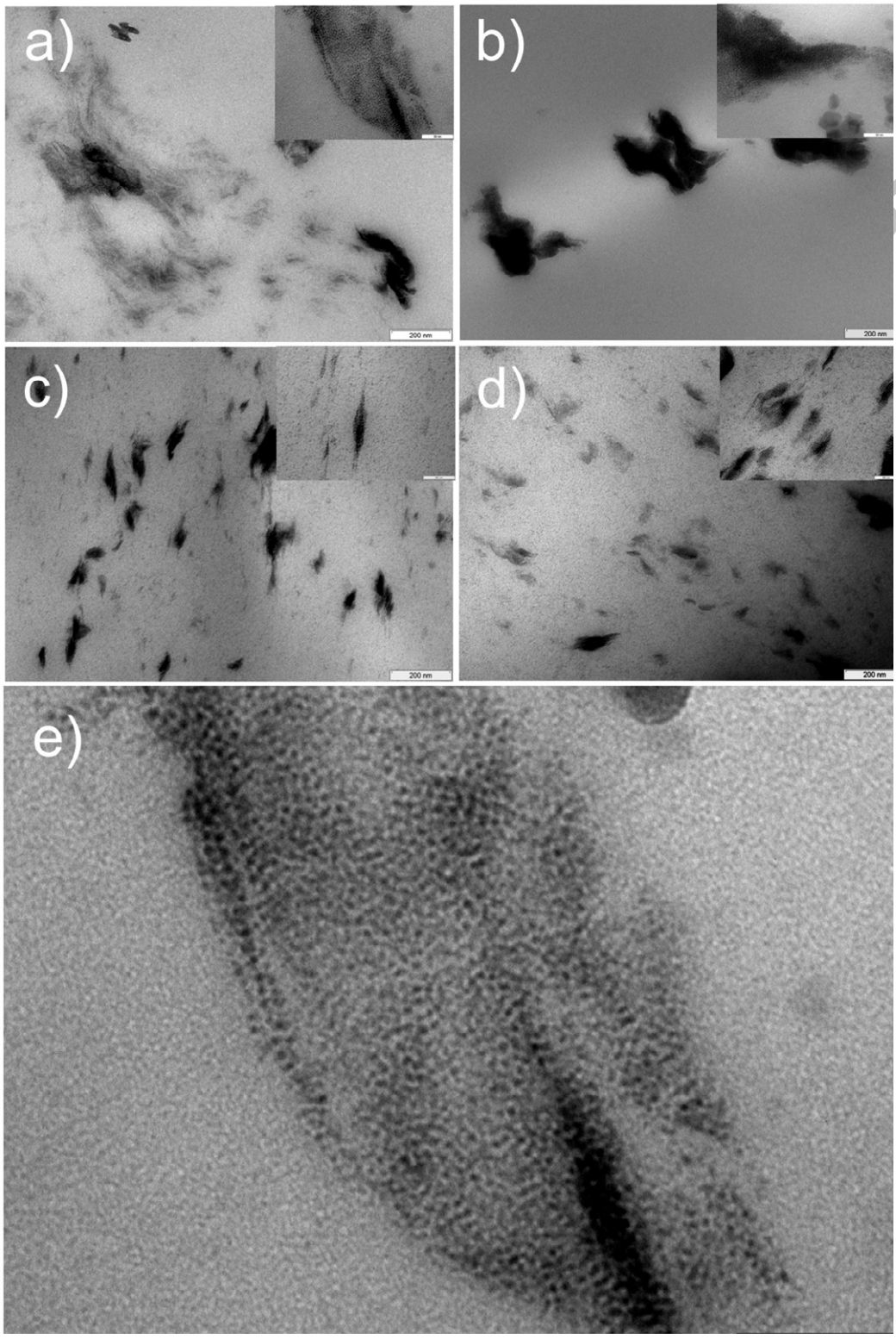
a)
b)
c)
d)
e)
200 nm
200 nm
200 nm
200 nm

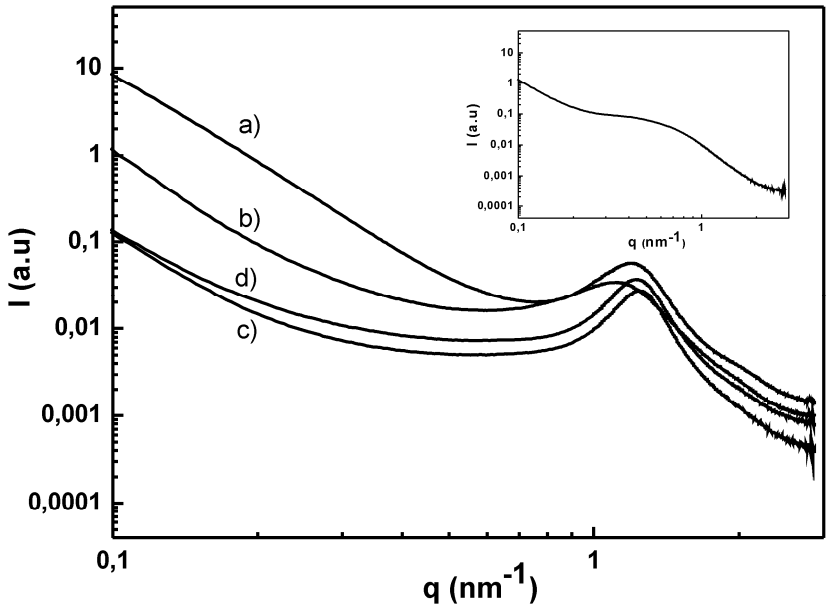

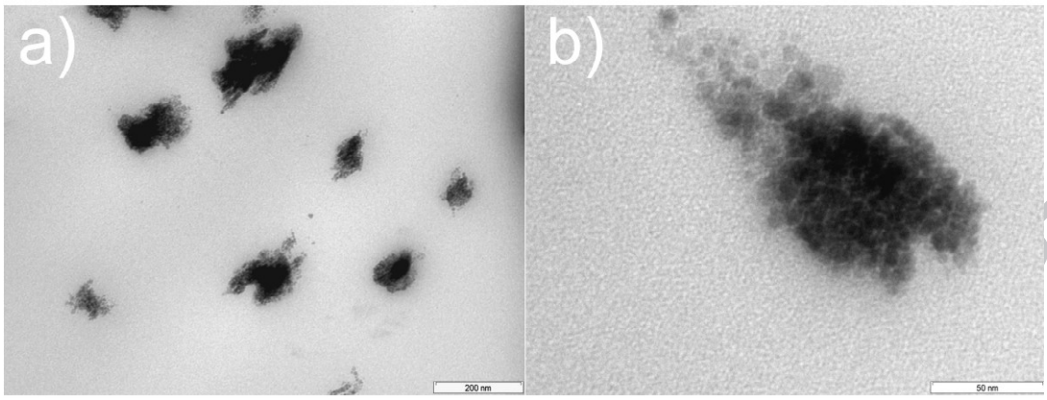

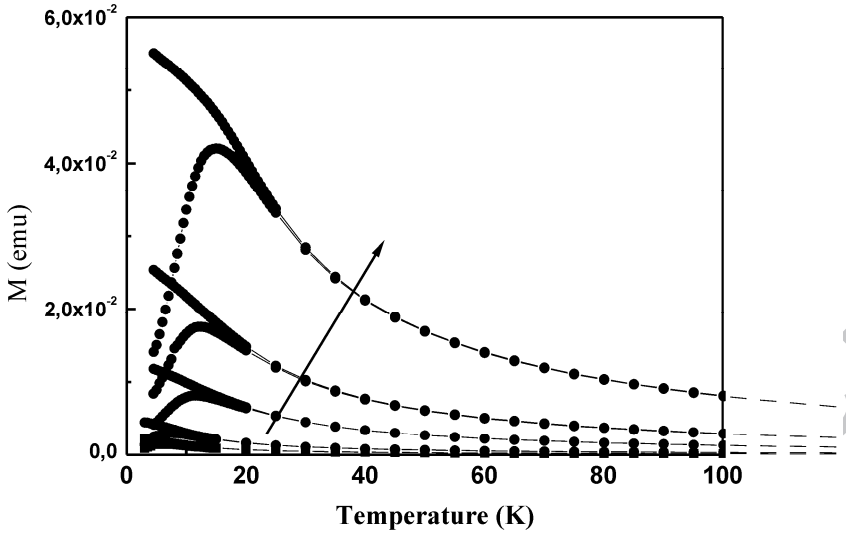

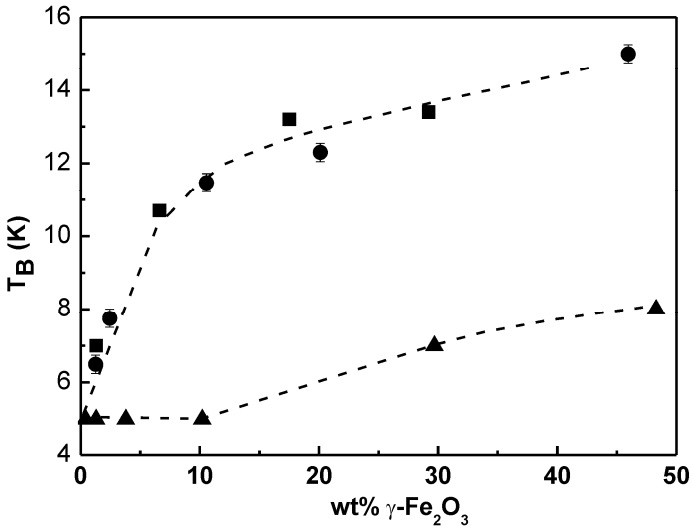

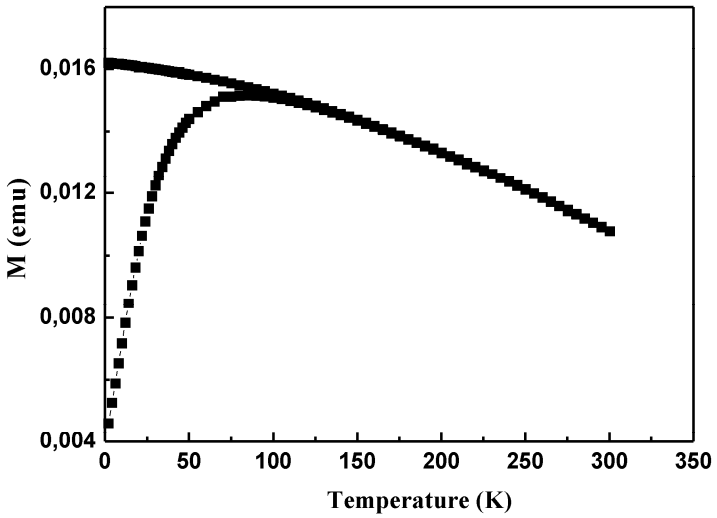

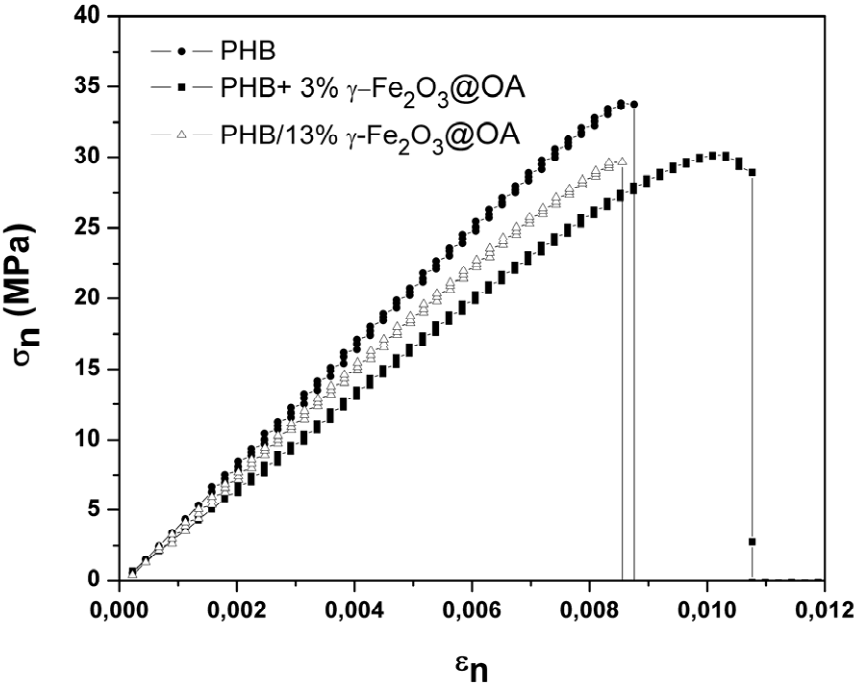
PHB
PHB+ 3% γ–Fe2O3@OA
PHB/13% γ-Fe2O3@OA
σn (MPa)
εn
0
5
10
15
20
25
30
35
40
0,000
0,002
0,004
0,006
0,008
0,010
0,012

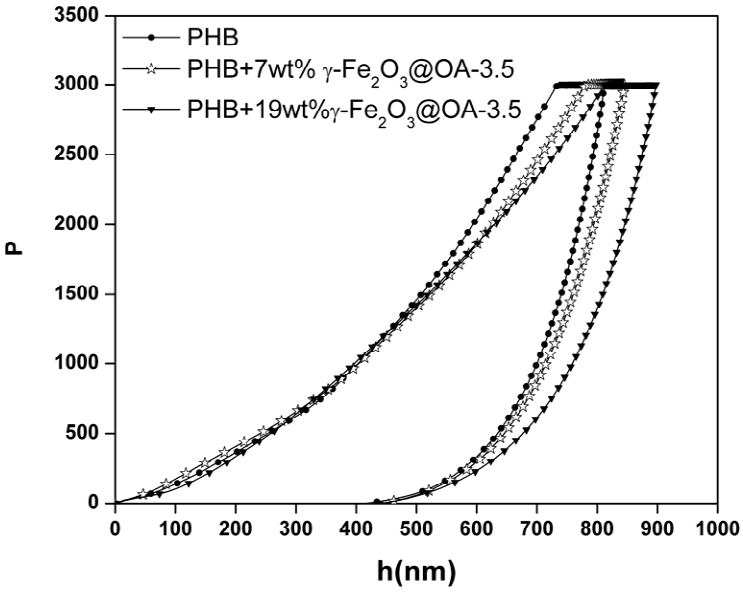
PHB
PHB+7wt% γ-Fe2O3@OA-3.5
PHB+19wt%γ-Fe2O3@OA-3.5
P
h(nm)
0
500
1000
1500
2000
2500
3000
3500
0
100
200
300
400
500
600
700
800
900
1000

51- Graphical abstract

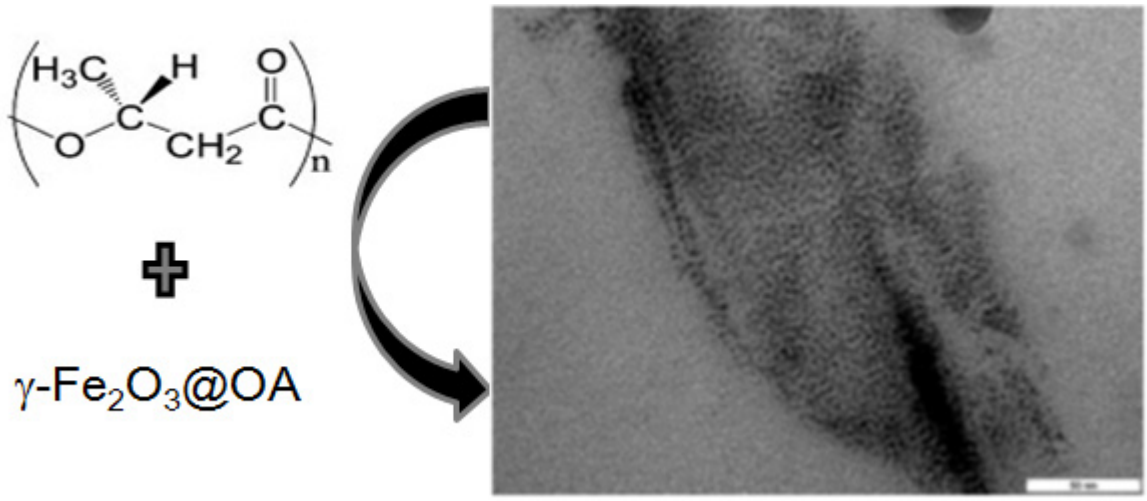

Highlights

- Superparamagnetic nanocomposites films were obtained from ultrafine NPs and PHB.
- NPs were segregated to the amorphous phase of PHB during crystallization.
- Magnetic properties were mainly controlled by number and size of dispersed clusters.
- NPs slightly improved the mechanical behaviour of PHB.
- NPs distribution was strongly controlled by crystallization of the PHB.

Table 1. Average size of clusters for different NPs contents in the matrix.

Sample	Mean Average Size (nm)
3.5 wt% ¡-Fe_2O_3@OA-3.5	91±64
7.0 *wt% ¡-Fe_2O_3@OA-3.5*	222±221
7.0 *wt% ¡-Fe_2O_3@OA-9.5*	131±93
13.0 *wt% ¡-Fe_2O_3@OA-3.5*	64±57
19.6 *wt% ¡-Fe_2O_3@OA-3.5*	85±86

Table 2. Thermal analysis results: Matrix crystalline fraction (Xc), peak melting temperature (Tm) and values obtained by DSC and average size of crystallites obtained by Scherrer equation of PHB nanocomposites films.

Sample	Xc (%) (Eq.1)	T_m (ºC)	Lamellar Thickness (Å)
0 *wt% ¡-Fe_2O_3@OA*	64.3	175.6	194
3.5 wt% ¡-Fe_2O_3@OA-3.5	65.7	176.6	203
7.0 *wt% ¡-Fe_2O_3@OA-3.5*	67.2	176.5	186
7.0 *wt% ¡-Fe_2O_3@OA-9.5*	66.9	176.4	--
13.0 *wt% ¡-Fe_2O_3@OA-3.5*	64.6	177.6	151
19.6 *wt% ¡-Fe_2O_3@OA-3.5*	64.8	176.1	149

Table 3. Mechanical properties of PHB/γ-Fe_2O_3@OA-3.5 nanocomposites.

	Uniaxial Tensile			Indentation		
Material	*E* (GPa)	σ_b (MPa)	ε_b (%)	E_r (GPa)	*H* (GPa)	P/S^2
0 *wt% γ-Fe_2O_3@OA*	4.13±0.15	32.96±2.20	0.92±0.12	6.18±0.63	0.28±0.05	5.08±0.49
3.5 *wt% γ-Fe_2O_3@OA-3.5*	3.50±0.39	28.04±3.11	0.98±0.03	6.09±0.81	0.27±0.06	5.24±0.46
7.0 *wt% γ-Fe_2O_3@OA-3.5*	--	--	--	5.05±0.27	0.26±0.03	6.99±0.43
13.0 *wt% γ-Fe_2O_3@OA-3.5*	3.96±0.37	28.94±3.36	0.87±0.07	5.04±0.38	0.23±0.03	7.22±0.71
19.6 *wt% γ-Fe_2O_3@OA-3.5*	3.63±0.14	27.33±5.00	0.83±0.13	4.70±0.33	0.19±0.02	6.67±0.66